Electronic Supplementary Material (ESI) for Soft Matter

Supplementary information: The role of the electrostatic double layer interactions in the formation of nanoparticle ring-like deposits at driven receding contact lines

Carmen L. Moraila-Martínez
Miguel A. Cabrerizo-Vílchez
Miguel A. Rodríguez-Valverde

November 18, 2012

S1 Roughness of the substrates

The roughness of the substrates was measured from the images acquired with a white light confocal microscope (PLμ, Sensofar Tech S.L.) using different objectives: 10X (1.39 x 1.02 mm^2), 20X (695.5 x 509.18 μm^2), 50X (285 x 209.2 μm^2), 100X (138.7 x 101.85μm^2) and 150X (95 x 69.75μm^2). As well, the roughness was measured with an atomic force microscope (MultiMode Scanning Probe Microscope, Nanoscope IV, Veeco). As expected, depending on the observation scale, quite different values of roughness were obtained (see Figure S1 and S2). Roughness parameters increased as the measurement scale because at lower scale, they revealed short range correlated features and at greater scales, they monitored entirely the long period roughness oscillations.

S2 Contact angle hysteresis of the substrates

Wettability is a very important property of solid surfaces, which is governed by both chemical composition and surface topography. Contact angle hysteresis of the substrate can provide the force necessary to pin the contact

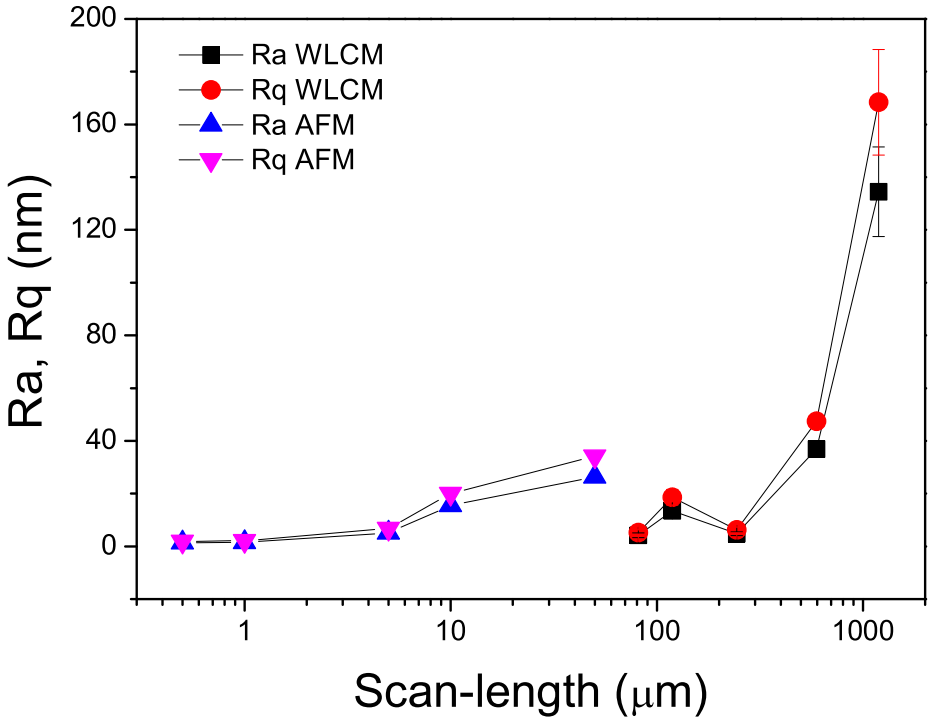

Figure S1: Roughness values of the PMMA substrates measured with White Light Confocal Microscopy (WLCM) and Atomic Force Microscopy (AFM).

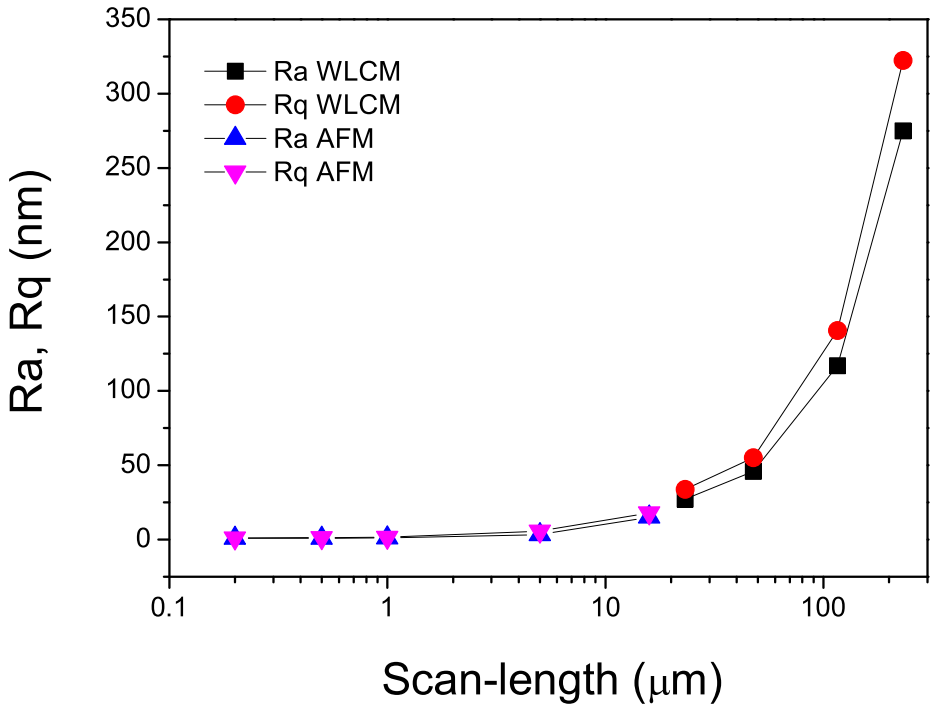

Figure S2: Roughness values of the TiO2 substrates measured with White Light Confocal Microscopy (WLCM) and Atomic Force Microscopy (AFM).

line. Therefore, the substrate hysteresis plays a very relevant role in the particle deposit formation. To investigate if the wetting response of PMMA and TiO2 was altered by pH, we performed low-rate dynamic contact angle experiments[1] with buffered drops at pH ranging from 2 to 9. The drop volume was 120μl. From the results plotted in Figure S3, we concluded that the advancing and receding contact angles of buffered drops on PMMA surfaces were independent of pH. Instead, for the case of TiO2 surfaces (Figure S4), the advancing and receding contact angles were dependant on the pH of the solution. This dependence might reflect the electrical response of the TiO2 in terms of the medium pH. The use of buffered solutions is justified with TiO2 surfaces.

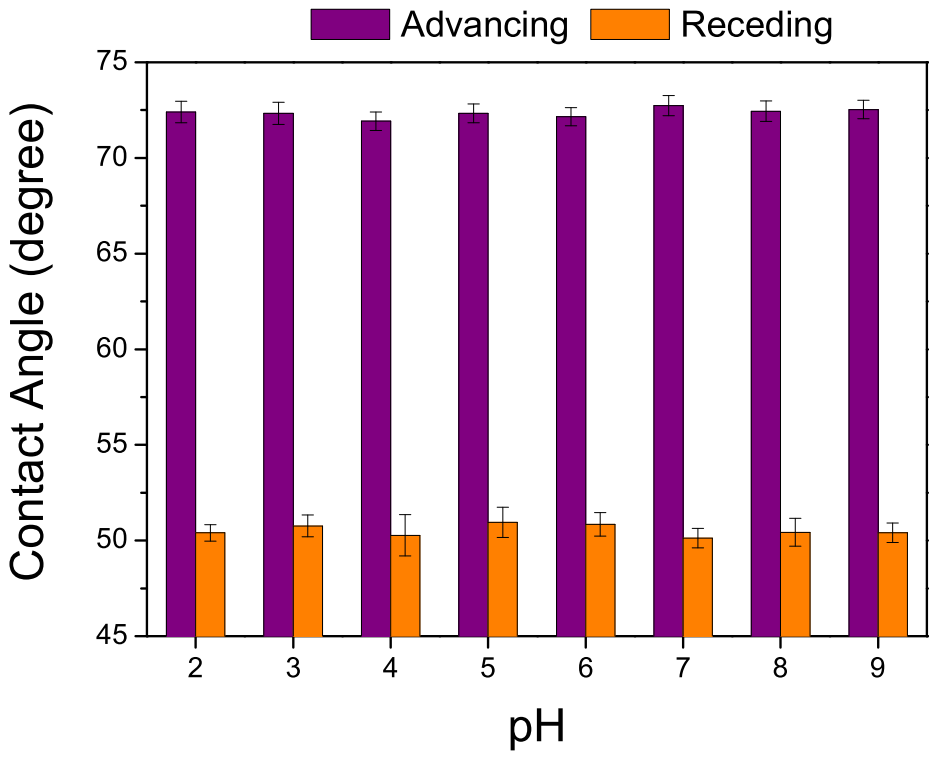

Figure S3: Advancing and receding contact angles measured on the PMMA surfaces as function of pH. The maximum drop volume was 120μl.

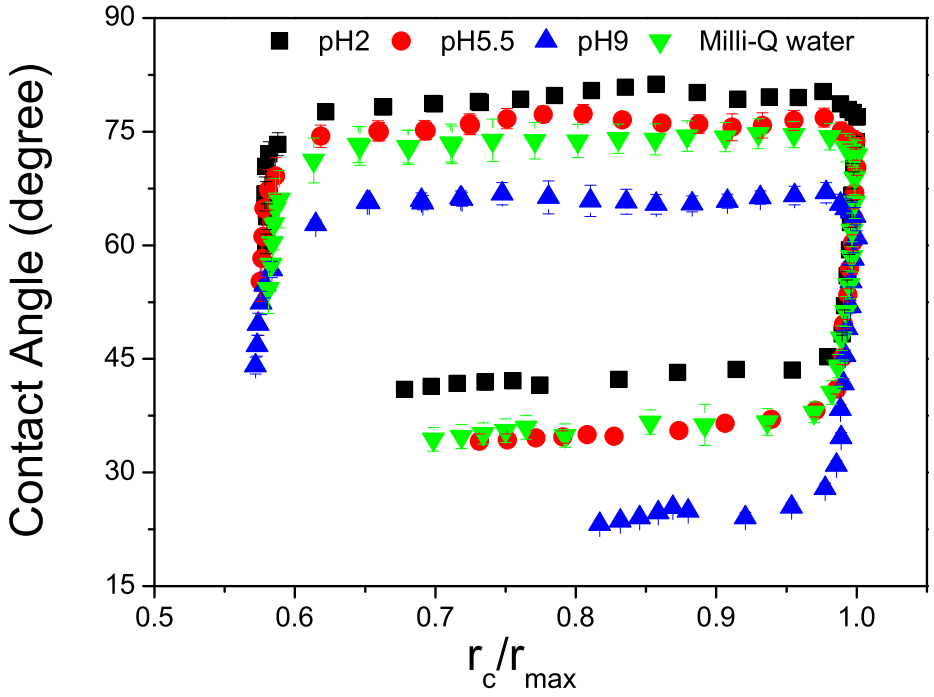

Figure S4: Advancing and receding contact angles measured on the TiO2 surfaces with Milli-Q water and buffer solutions at pH2, pH5.5 and pH9. The maximum drop volume was 120μl.

S3 Implementation of the Controlled Shrinking Sessile Drop method

Generally, the evaporation of sessile drops occurs in two distinct modes: at a constant contact radius and decreasing contact angle and next, at a constant contact angle and decreasing contact radius. During the evaporation of a sessile drop, the triple contact line of the drop can be "pinned" to the surface, due to contact angle hysteresis. This pinning prevents the drop from receding and so, the drop contact radius remains constant. Just before the backward movement of contact line, a receding contact angle is hold. The amplitude of contact angle hysteresis and the receding contact angle of the substrate will determine the transition of an evaporating drop from the situation of static contact line to moving contact line with constant contact angle. In practice, the reproducibility of experiments with evaporating drops is very poor. Kinetics of evaporating drop is very long since evaporating drops undergo a minimum rate of liquid loss. Furthermore, there is a strong influence on the receding contact angle value from the rate of liquid removal from the drop.

It is known that the evaporation time is proportional to the initial drop volume. For the case of drop evaporation in saturated vapor and constant contact angle, it has also been reported that the liquid-vapour area, A_{LV}, decreases linearly with time[2,3]. If a sessile drop is slowly shrinking with constant contact angle, the following rule should be hold neglecting thermal and Marangoni effects:

$$\frac{dA_{LV}}{dt} = \frac{dA_{SL}}{dt}\cos\theta_r \tag{S1}$$

where A_{SL} is the solid-liquid area and θ_r, the receding contact angle. From Eq. S1, if $A_{LV} \propto (t_p - t)$ then $r_c^2 \propto (t_p - t)$, as well. The time t_p (pinning time) stands for the transition time between the fixed contact line mode and the constant contact angle mode. For spherical drops, the volume scales with contact radius as $V \propto r_c^3$[1]. If this scaling applies to gravity-flattened drops, we predict that $V \propto (t_p - t)^{3/2}$ for the constant contact angle mode of drop evaporation. In fact, this result agrees with the evaporation rate of a receding drop[2]:

$$-\frac{dV}{dt} \propto \sqrt{t_p - t} \tag{S2}$$

whereas the loss rate of volume for a sessile drop with fixed contact line is:

$$-\frac{dV}{dt} = const. \tag{S3}$$

The first stage of drop evaporation (constant contact radius) is better reproduced at quadratic flow rate rather than at constant flow rate, following the law:

$$V(t) = V_0 + V_{\max} + V_{\max}\left(1 - \frac{t}{t_p}\right)^3 \tag{S4}$$

where V_0 is the volume of the "seed" drop, $V_{\max}$ is the maximum volume of liquid removed from the drop and t_p is the pinning time (programming details are shown in ref.[1]). Typical values were $V_0 = 20\mu$l and $V_{\max} = 100\mu$l. This volume variation adequately reproduces the pinning behaviour of the evaporating drop because it standardizes the impeding motion of the drop on the substrate, giving reproducible receding contact angles. The next stage at constant contact angle (i.e. linearly decreasing liquid-vapor area) is described as the law:

$$V(t) = V_0 + V_{\max} - V_{\max}\left(\frac{t}{t_p} - 1\right)^{\frac{3}{2}}\left(\frac{t_t}{t_p} - 1\right)^{-\frac{3}{2}} \tag{S5}$$

where t_t is the total time. Eq. S5 is valid for $t > t_p$ and it connects to Eq. S4 at $t = t_p$. The drop volume in terms of time in an ideal CSSD experiment is illustrated in Figure S5. The CSSD method is further able to reproduce the final mixed stage of evaporating drops[2], where the flow is accelerated. Unlike freely-evaporating drops of pure liquids, the receding contact lines of shrinking drops mostly held a constant contact angle over a significant area. The actual drop volume agreed with the volume suctioned by the microinjector (as Eqs. S4 and S5), without significant macroevaporation.

In fast CSSD experiments (t_t = 100s), no hydrodynamics effects were found. The CSSD method was independent on the process length below t_t =900s. Above 900s, the shrinking drop began to evaporate significantly because the withdrawal rate was similar to the actual evaporation rate.

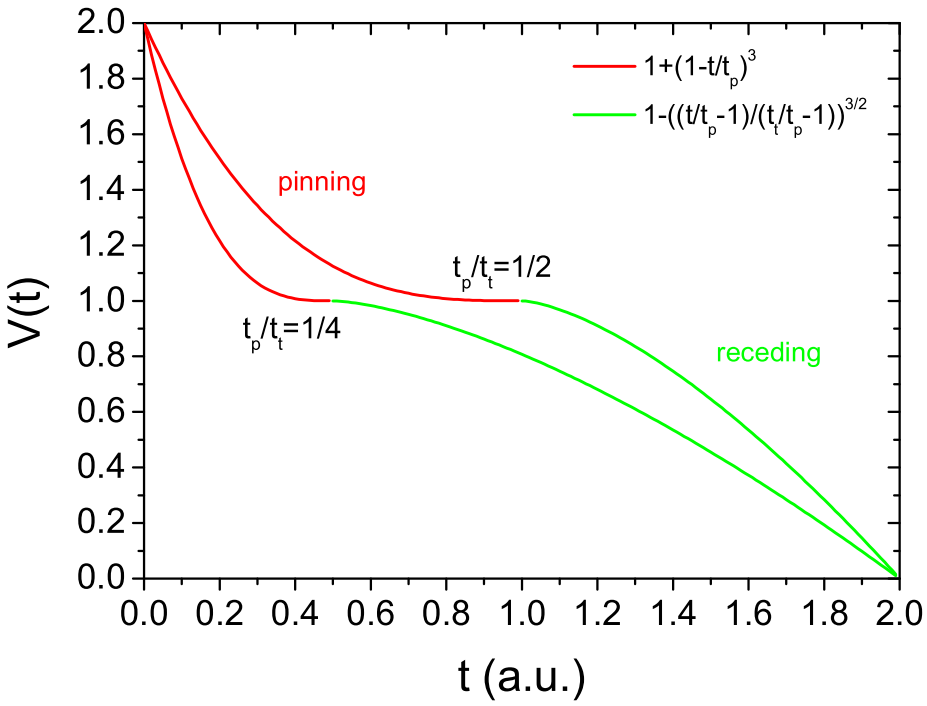

Figure S5: Drop volume in terms of time in CSSD experiments. The time t_p symbolizes the pinning time and the time t_t, the length of the process ($V_0 = 0$,$V_{\max} = 1$).

S4 Optical microscopy monitoring of the contact line of evaporating drops

Although no aggregation/sedimentation was detected in suspension at $\Phi_V = 1\%$, we observed particle/particle shear-enhanced aggregation in free evaporation experiments. We monitored with optical microscopy the triple line of freely-evaporating drops of 5μl containing SiO2 particles (1.16μm diameter, Microparticles) buffered at pH2 and pH9 at $\Phi_V = 0.01\%$ on PMMA substrates. We used micron-size spheres because they are routinely used to monitor the liquid flow in evaporating drops with optical microscopy. The entire evaporation process was monitored in-situ using an optical microscope (Optiphot-2, Nikon) with a 20X objective. The results showed that the accumulation of microparticles at the contact line was different as the pairwise electrostatic interactions (see Movies S6 and S7-Acceleration x 24). With strong particle-particle repulsion (pH9, Movie S6), single particles accumulated at the contact line from the beginning of the process. They moved together with the receding contact line until a global pinning event occurred and finally, the drop entirely evaporated. Instead, with weak particle-particle repulsion (pH2, Movie S7), visible particle aggregates accumulated at the contact line and local events of (self-)pinning occurred earlier than for strongly interacting particles (see the diameter of the final ring-like deposits formed with SiO2-90 in Figure 2). This is an evidence for the shear-induced aggregation. From the "rush-hour effect" reported by Marin et al.[4], the order-to-disorder transition in the deposits occurred earlier with weaker interparticle repulsion although it is apparently easier to arrange non-interacting particles.

We also monitored the contact line of CSSDs with the SiO2-120 suspension buffered at pH2 and pH9 at $\Phi_V = 1\%$ on PMMA substrates. The entire CSSD experiment was also monitored in-situ using the same optical microscope but with a 10X objective. Although the nanoparticles were not visible due to their smaller size, with weak particle-particle repulsion (pH2) we observed how a ring-like deposit was completed during the first pinning event of the contact line. Instead, with strongly interacting particles (pH9), no particle deposits were left during the entire CSSD experiment except for the remaining central spot. The contact line dynamics observed by optical microscopy with both systems validated the results shown in Figures 7 and 8. It is plausible to assume that weakly interacting nanoparticles also underwent

orthokinetic aggregation.

References

[1] C. L. Moraila-Martínez, F. J. M. Ruiz-Cabello, M. A. Cabrerizo-Vílchez and M. A. Rodríguez-Valverde, *Colloids Surf., A*, 2012, **404**, 63 – 69.

[2] H. Y. Erbil, *Adv. Colloid Interface Sci.*, 2012, **170**, 67–86.

[3] M. Sokuler, G. K. Auernhammer, C. J. Liu, E. Bonaccurso and H.-J. Butt, *Europhys. Lett.*, 2010, **89**, 36004.

[4] A. G. Marin, H. Gelderblom, D. Lohse and J. H. Snoeijer, *Phys. Fluids*, 2011, **23**, 091111–1.